# Lab Notes

**Editors**

Thomas M. Moses | Shane F. McClure
Sally Eaton-Magaña | Artitaya Homkrajae

*Figure 1. This 1.02 ct modified pear portrait-cut natural diamond has a checkered pattern on the flat pavilion, created using a laser. Photo by Gaurav Bera and Tejas Jhaveri; field of view 7.10 mm.*

## Checkered Pattern on DIAMOND

Recently, the Mumbai laboratory received a modified pear portrait-cut natural diamond weighing 1.02 ct and measuring 6.98 × 5.82 × 2.33 mm. A portrait cut consists of a flat crown and a flat pavilion, creating the appearance of a picture frame. The flat pavilion facet was fashioned with a checkered design using a laser (figure 1). This unique fashioning was done intentionally to enhance the appearance of the diamond. Therefore, it did not impact the diamond's clarity, polish, and symmetry grading.

Standard gemological testing, including microscopic examination, proved that this was a laser-fashioned pattern, and no evidence of clarity or color enhancement was observed. Natural inclusions such as twinning wisps were present, and an $SI_1$ clarity grade and H color were assigned.

*Tejas Jhaveri*

## Rare GADOLINITE Gemstone

GIA's Tokyo laboratory recently received a 22.33 ct black faceted stone measuring 18.19 × 13.05 × 11.05 mm (figure 2). The stone was nearly opaque, and it was difficult to observe internal inclusions and growth features. Numerous fractures and reflective fingerprints were observed over the entire surface, which showed a very dark green bodycolor with LED fiber-optic lighting under magnification. Metallic minerals with a yellow color were exposed on the surface along fractures (figure 3). The stone had a hydrostatic specific gravity of 4.25. The refractive index ranged from 1.770 to an over-the-limit reading with 1.81 RI liquid, giving a birefringence of at least 0.040.

*Figure 2. A 22.33 ct oval mixed-cut gadolinite exhibiting a very dark and almost opaque bodycolor and multiple fractures covering the surface. Photo by Shunsuke Nagai.*

*Editors' note: All items were written by staff members of GIA laboratories.*

Gems & Gemology, Vol. 61, No. 1, pp. 58–71.

© 2025 Gemological Institute of America

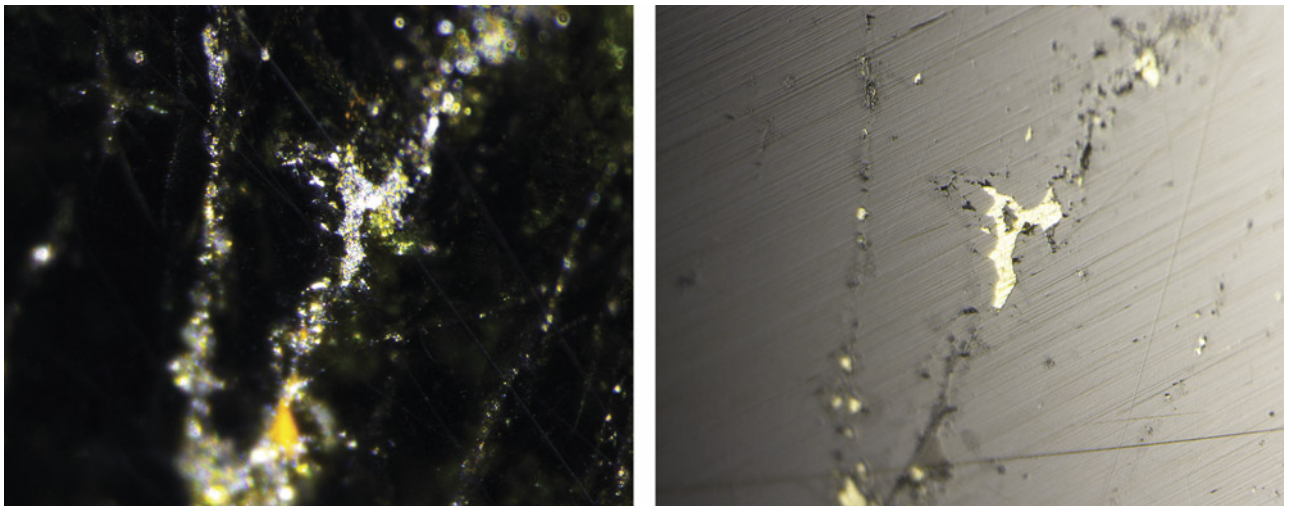

*Figure 3. Left: A surface-reaching fracture in gadolinite observed with fiber-optic illumination. The fracture is filled with a reflective material. Right: The same fracture observed under reflective lighting. The yellowish fracture-filling material shows a metallic luster. Photomicrographs by Yusuke Takamura; field of view 1.04 mm.*

Raman spectroscopy using 532 nm laser excitation showed a broad band around 900 $cm^{-1}$ and a match to the RRUFF reference spectrum for gadolinite-(Y) (B. Lafuente et al., 2015, https://rruff.info/about/downloads/HMC1-30.pdf). Laser ablation–inductively coupled plasma–mass spectrometry was performed, revealing that the stone contained ytterbium, iron, beryllium, silicon, and rare earth elements (REEs) such as dysprosium and erbium, which is characteristic for gadolinite. The stoichiometric composition of the stone was calculated to be Y = 1.52, the sum of other REEs = 0.42, Fe = 0.80, Be = 1.82, and Si = 2.23, assuming a stoichiometric amount of O = 10. This result closely matched the formula of gadolinite and identified gadolinite-(Y) ($Y_2Fe^{2+}Be_2(Si_2O_{10})$) as the predominant composition. The stone's standard gemological properties, Raman spectroscopic features, and stoichiometry indicated gadolinite-(Y).

Gadolinite-(Y) is a rare mineral species that occurs in metasomatically altered acidic igneous rocks or complex alkaline granite pegmatites (L. Nasdala et al., "Metamict gadolinite-(Y) from Ratnapura, Sri Lanka," *Journal of the Geological Society of Sri Lanka*, Vol. 24, No. 1, 2023, pp. 23–30). Gadolinite can also be obtained from sedimentary deposits along with gem species such as corundum, chrysoberyl, spinel, garnet, tourmaline, topaz, and zircon (C.B. Dissanayake and M.S. Rupasinghe, "Application of geochemistry to exploration for gem deposits, Sri Lanka," *Journal of Gemmology*, Vol. 23, No. 3, 1992, pp. 165–175). Though rarely used as a faceted gemstone, gadolinite is of interest to collectors (E.A. King Jr., "Texas Gemstones," Bureau of Economic Geology, Report of Investigations No. 42, University of Texas at Austin). To our knowledge, this is the first time gadolinite has been submitted to GIA.

*Yusuke Takamura and Kazuko Saruwatari*

## LABORATORY-GROWN DIAMONDS

### CVD-Grown Diamond with an Unusual Blue Band

A 1.09 ct D-color diamond grown by chemical vapor deposition (CVD) was recently submitted to the Mumbai laboratory. This submission displayed an interesting blue band, seen through the pavilion facets (figure 4). The blue band could not be observed through the table facet. Infrared spectroscopy showed that it was type IIb with a bulk

*Figure 4. A blue growth band can be seen through the pavilion (but not face-up) in this 1.09 ct HPHT-treated CVD-grown diamond. Photo by Gaurav Bera.*

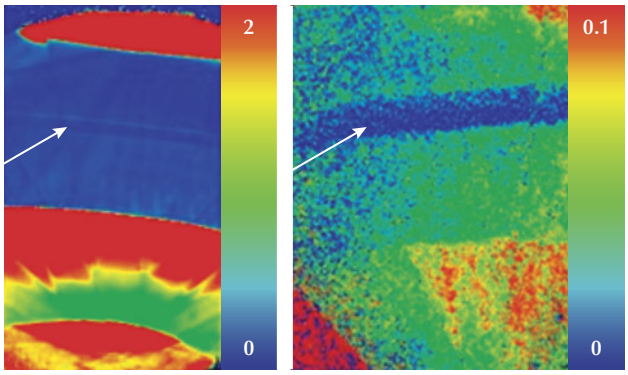


*Figure 5. False-color PL maps showing normalized peak intensities (normalized using the diamond Raman line). These were collected using 532 nm excitation to document the $SiV^-$ doublet at 736.6/736.9 nm (left) and 455 nm excitation to document the H3 defect at 503.2 nm (right). The region corresponding to the blue band is indicated by an arrow.*

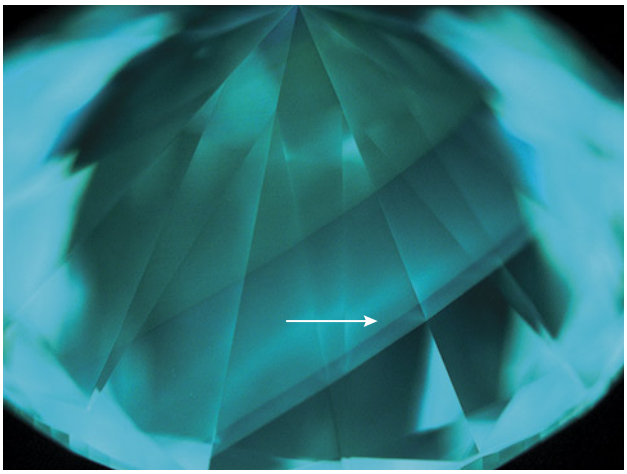

*Figure 6. DiamondView imaging of the pavilion of the 1.09 ct diamond. The fluorescence color was consistent with HPHT-treated CVD-grown diamond. The region corresponding to the blue band is indicated by an arrow.*

uncompensated boron concentration of ~10 ppb; the observed color was likely due to boron and a higher concentration of uncompensated boron within this blue growth layer.

Boron is present in only about 5% of CVD-grown diamonds, with the 2800 $cm^{-1}$ infrared absorption band indicating the presence of uncompensated boron (S. Eaton-Magaña et al., "Laboratory-grown diamonds: An update on identification and products evaluated at GIA," Summer 2024 *G&G*, pp. 146–167). However, the detected boron concentration is generally <20 ppb, too low to impart blue color. Additionally, thin layers of boron-doped CVD overgrowth on natural diamond have had a high enough concentration to impart a blue color appearance to the combined CVD/natural hybrid stone (e.g., Summer 2017 Lab Notes, pp. 237–239). Nevertheless, boron has not been a common cause of blue color in CVD-grown diamonds, unlike their HPHT-grown counterparts produced through high pressure and high temperature.

Besides boron impurities, the $SiV^0$ center at 946 nm has been shown to create blue color in CVD diamonds (U.F.S. D'Haenens-Johansson et al., "CVD synthetic gem diamonds with high silicon-vacancy concentrations," *Conference on New Diamond and Nano Carbons*, May 2015, Shizuoka, Japan). However, photoluminescence (PL) mapping indicated this region showed lower silicon (as $SiV^-$ at 737 nm), eliminating silicon as the likely cause of the blue color (figure 5, left).

PL spectroscopy and DiamondView imaging (figure 6) established that this CVD-grown diamond had been subjected to post-growth HPHT annealing. Spectroscopic features supporting this conclusion include several sharp peaks in the 520–580 nm wavelength range (using 514 nm excitation) that develop in CVD-grown diamonds following HPHT treatment (W. Wang et al., "CVD synthetic diamonds from Gemesis Corp.," Summer 2012 *G&G*, pp. 80–97). Pronounced greenish blue phosphorescence was also detected with DiamondView imaging.

No known boron-related features, such as the 648.2 nm peak (attributed to a boron interstitial), were detected by PL mapping using 455 and 532 nm laser excitation within the region corresponding to the blue band (figure 5, left). However, this lack of boron-related PL features is not surprising, as the 648.2 nm peak often does not develop unless the laboratory-grown diamond has been subjected to irradiation and subsequent annealing treatment (B.L. Green, "Optical and magnetic resonance studies of point defects in single crystal diamond," PhD thesis, University of Warwick, 2013). PL mapping with 455 nm excitation (figure 5, right) did indicate that the region with the blue band showed a pronounced decrease in the H3 defect ($NVN^0$). The thickness of this region with low nitrogen impurities was ~300 μm and corresponded with the blue-colored area.

When boron impurities are present but electrically compensated by other defects such as nitrogen, the 2800 $cm^{-1}$ peak would be undetected or detected at lower concentrations. It is unclear whether this blue layer with a sufficiently high concentration of uncompensated boron to show color was intentionally created by the manufacturer or resulted from an accidental disruption of the standard growth recipe.

*Sally Eaton-Magaña, Manisha Bhoir, and Priyanka Kadam*

## CVD Laboratory-Grown Gem Diamonds from Plasmability

Chemical vapor deposition (CVD) technology has been widely used to grow diamonds for the jewelry market, targeting popular colors and sizes. The majority of these

*Figure 7. Three large CVD-grown diamonds submitted by Plasmability to GIA for scientific examination: A matching pair of pear-cut gems weighing 8.88 and 8.89 ct, as well as a 10.13 ct round brilliant. These American-grown diamonds are displayed with a U.S. quarter (24.26 mm diameter) for scale. Photo by Jian Xin (Jae) Liao.*

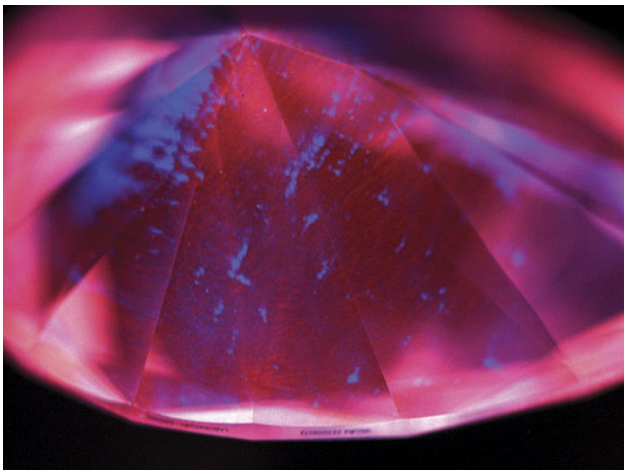

*Figure 8. Representative deep-UV fluorescence image of a 2.90 ct CVD diamond from Plasmability, collected using the DiamondView. The image is dominated by red–orange fluorescence from $NV^0$ centers, a common feature for untreated CVD laboratory-grown diamonds, along with irregular blue fluorescing dislocation bundles. No growth layers were observed, indicating that it was produced through a single uninterrupted growth cycle. Image by Madelyn Dragone.*

products are colorless to near-colorless, with a smaller proportion being fancy colored. Producers often rely on post-growth treatment for color improvement, with most colorless and near-colorless CVD diamonds having undergone high-pressure, high-temperature (HPHT) annealing (S. Eaton-Magaña et al., "Laboratory-grown diamond: A gemological laboratory perspective," *Journal of Gems & Gemmology*, Vol. 23, No. 6, 2021, pp. 25–39). Faceted CVD gem diamond sizes span from melee to tens of carats. It is challenging to grow thick samples without crystal quality degradation. Thus, most sizeable gems are produced through multiple CVD growth stages, resulting in layered growth structures. Close to 10 growth steps have been reported in some CVD diamonds tested at GIA (e.g., Summer 2023 Lab Notes, pp. 213–214). Here we report on colorless and near-colorless CVD gem diamonds from the Texas-based company Plasmability, which were produced by single-step growth up to 9 mm in thickness and were not subjected to post-growth treatment.

Recently, GIA tested a few thousand laboratory-grown diamonds manufactured by Plasmability. The sizes ranged from about half a carat to more than 10 carats (figure 7). Approximately 85% were colorless, with the rest being near-colorless. Clarity grades varied from VS to VVS. Deep-UV fluorescence imaging is an effective technology for studying diamond growth history, since different growth sectors or growth interruptions will create discontinuities in fluorescence features. Deep-UV fluorescence images collected using the DiamondView were inspected for several hundreds of samples. They were dominated by red–orange emission from $NV^0$ centers, with irregular patches of dislocation bundles, associated with blue band-A fluorescence (figures 8 and 9). No growth layers were observed for tested samples, confirming that they were produced by a single growth step. Excluding the dislocation bundles, the fluorescence was homogeneous, evidence that remarkable control was maintained over the various CVD conditions, including temperature, gas composition, pressure, and power throughout the growth period. Any fluctuations in these parameters would otherwise lead to detectable changes in impurity uptake, typically resulting in interfaces parallel to the growth plane. Complementary cathodoluminescence imaging of a selection of the largest diamonds confirmed these observations (figure 9). A review of gem-quality CVD laboratory-grown diamonds submitted to GIA to date weighing 8.00 ct or more has shown that fewer than 1% were grown without interruption, the largest being a 10.13 ct J-color specimen by Plasmability (figures 7 and 9).

Infrared absorption spectroscopy indicated that these were type IIa, typical for gem-quality CVD-grown diamonds. Most stones showed no absorption features from optical defects; however, very weak absorption at 3123 $cm^{-1}$ from $NVH^0$ was detected for only a few diamonds. Photoluminescence spectroscopy collected at liquid nitrogen temperature using 514 and 633 nm laser excitations revealed weak emissions at 596/597 nm, in addition to moderately strong emissions from $NV^0$ and $NV^-$ centers at 575 and 637 nm, respectively. A weak emission doublet at 736.6 and 736.9 nm due to $SiV^-$ was recorded in some samples. These observations strongly suggest that no post-growth treatment was applied and that they were as-grown crystals (U.F.S. D'Haenens-Johansson et al., "Synthesis of diamonds and their identification," *Reviews in Mineralogy and Geochemistry*, Vol. 88, 2022, pp. 689–753).

In summary, high-quality CVD-grown gem diamonds are produced by Plasmability using a single-step growth

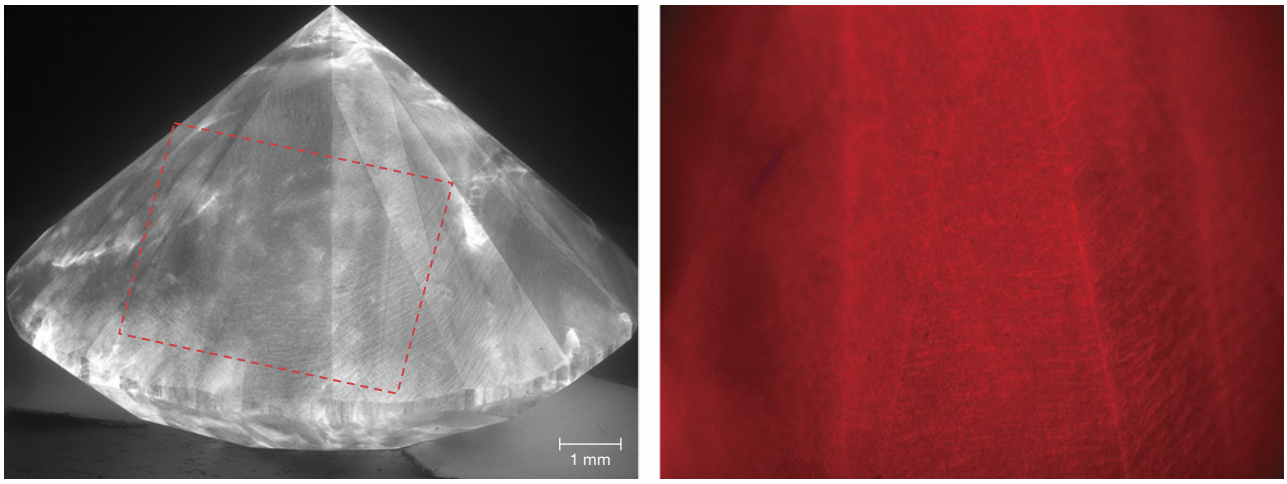


*Figure 9. The absence of distinct layers and interfaces in the cathodoluminescence (left) and deep-UV fluorescence (right) images for a 10.13 ct CVD laboratory-grown diamond by Plasmability confirms that it was produced by a single growth event. Fine linear striations can be observed, characteristic of step-flow growth. Images by Elina Myagkaya (left) and Ulrika D'Haenens-Johansson (right).*

process. Additionally, their colorless and near-colorless grades were achieved without post-growth treatment. This combination of features is rare in gem-quality CVD-grown diamonds.

*Ulrika D'Haenens-Johansson, Tingyen Yeh, Stephanie Persaud, Elina Myagkaya, Wuyi Wang, and Thomas Moses*

## Fancy Vivid Yellow HPHT-Grown Diamonds

GIA's Hong Kong laboratory recently received 26 yellow laboratory-grown diamonds, ranging from 1.03 ct to 2.32 ct with VVS to VS clarity. They were all color graded as Fancy Vivid yellow except for one that was Fancy Intense yellow. It had a very attractive yellow color with no other color components. As shown in figure 10, the diamonds were cut into different shapes: ovals, cushions, hearts, and a pear. These were undisclosed as laboratory-grown diamonds when submitted for examination. Examination confirmed that all were grown by high-pressure, high-temperature (HPHT).

Diamonds grown by the HPHT process have been commercially available since the mid-1990s (U.F.S. D'Haenens-Johansson et al., "Large colorless HPHT-grown synthetic gem diamonds from New Diamond Technology, Russia," Fall 2015 *G&G*, pp. 260–279). To produce yellow diamonds, isolated nitrogen is incorporated into the crystal. As the growth processes continue to improve, consistent production of larger size and better color diamonds is now possible (Winter 2016 Lab Notes, p. 416). The submission of these 26 laboratory-grown diamonds, which possessed a similar intensity of yellow color, caught our attention.

Fourier-transform infrared spectroscopy confirmed that 25 of the samples were type Ib diamonds, with a sharp peak at 1344 $cm^{-1}$ and a broader absorption at 1130 $cm^{-1}$ and no detectable A-center. The concentration of isolated nitrogen was within 4–16 ppm. Only one sample with Fancy Intense color showed an additional 2800 $cm^{-1}$ boron-related feature (3 ppb in $B^0$ concentration) in two orientations besides 1344 and 1130 $cm^{-1}$. This special sample was a mixed-type diamond. Since the concentration of isolated nitrogen

*Figure 10. Selection of Fancy Vivid yellow HPHT-grown diamonds, ranging from 1.03 ct to 2.32 ct. Photo by Johnny Leung.*

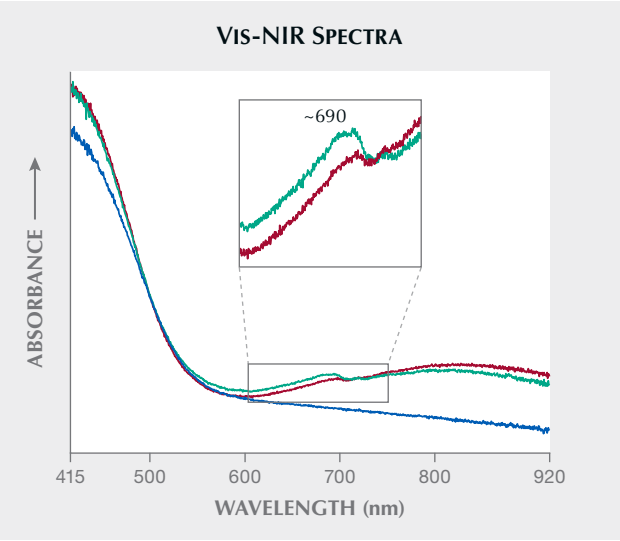


*Figure 11. Vis-NIR spectra of 26 samples. The blue line is a representative spectrum for 24 of the samples. The red and green lines are two samples with nickel-related defects. Spectra are offset vertically for clarity.*

determined the color of this diamond, it must be well controlled to produce an attractive, vivid yellow color.

Ultraviolet/visible/near-infrared (UV-Vis-NIR) spectroscopy showed a very strong absorption by isolated nitrogen occurring in the ultraviolet range and extending into the visible range, creating a yellow hue. Among the 26 samples, 24 showed very similar Vis-NIR spectra, represented by the blue curve in figure 11. Two showed slightly different Vis-NIR spectra (the red and green curves in figure 11), with the additional absorption at ~690 nm indicating nickel-related defects (W. Wang et al., "Natural type Ia diamond with green-yellow color due to Ni-related defects," Fall 2007 *G&G*, pp. 240–243).

Photoluminescence (PL) spectroscopy was conducted at liquid nitrogen temperature with several laser excitations. PL spectra features for these HPHT-grown diamonds were predominantly nitrogen-related defects. H3 was present in the 457 nm PL spectrum with varying intensities. Around half of the samples had moderate H3 intensity, and ~23% had strong H3. More than half showed H2 in the 830 PL spectrum. All these emission features were exceptionally sharp and consistent with HPHT growth with very low dislocations. Moreover, nitrogen vacancy centers ($NV^0$, $NV^-$) were present in the 514 nm spectrum. Approximately 73% of the samples showed an 882.7/884.4 nm doublet in 830 nm PL from the well-known nickel-related defect. (Two samples showed an extremely strong 883/884 nm doublet; these same two showed a 690 nm peak in the Vis-NIR spectrum.)

Fluorescence images collected using the DiamondView revealed a distinctive cuboctahedral growth pattern typical of HPHT-grown diamond (figure 12). The strong green fluorescence color observed was due to the presence of H3. This color is different from the weak green/yellow fluorescence of natural type Ib diamond. Green phosphorescence was also detected.

Microscopic examination with crossed polarizers revealed no strain patterns (anomalous birefringence) except for small strain fields around some metallic flux inclusions. Lack of strain indicates a very low dislocation density, which is also a characteristic of HPHT-grown diamonds. Magnification exposed the presence of color zoning with a banded structure. Also observed were some pinpoints and fractures.

All 26 stones were concluded as HPHT-grown diamonds with similar gemological properties. To consistently produce this attractive Fancy Vivid yellow color, isolated nitrogen concentration, temperature and pressure, and growth environment must be carefully controlled.

*Figure 12. DiamondView imaging of two of the diamonds revealed cuboctahedral growth patterns and green fluorescence. Images by Ka Wing Tam and Wing Hin Choi.*

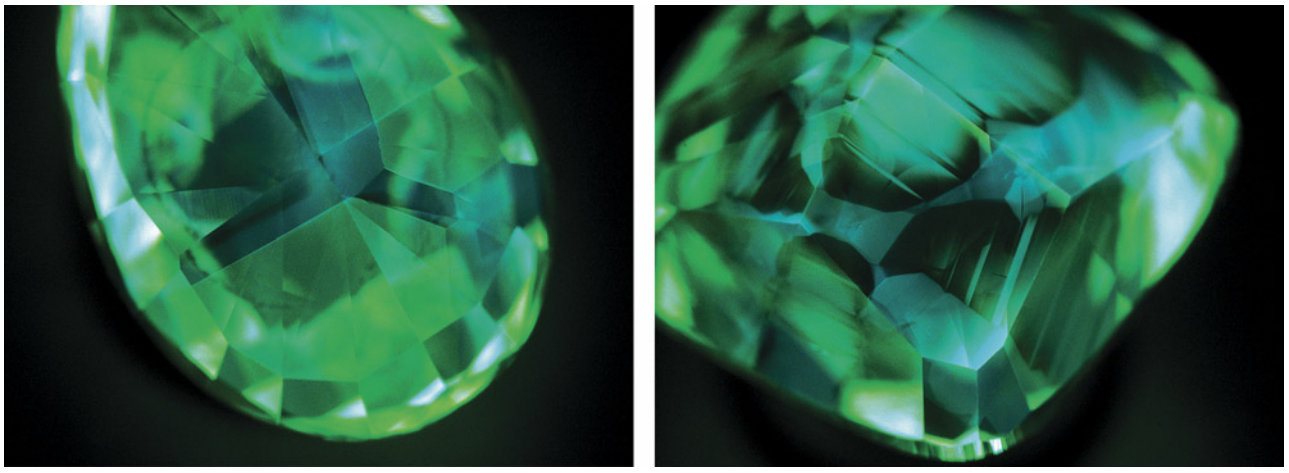

This indicates that the manufacturer knew the growth parameters to produce these attractive yellow diamonds.

*Suet Man Yau and Terry "Ping Yu" Poon*

### Black OPAL with Unique Play-of-Color

The Carlsbad laboratory recently examined a black oval cabochon displaying play-of-color, set in a white metal ring with 24 near-colorless round brilliants (figure 13). The stone measured approximately 19.56 × 14.28 × 3.00 mm. Standard gemological testing revealed a spot refractive index of 1.44, as well as weak blue long-wave fluorescence, very weak blue short-wave fluorescence, and weak green phosphorescence. These gemological properties were consistent with Australian black opal.

The visual impact of this opal was particularly striking, displaying vivid orange play-of-color when viewed face-up and brilliant flashes of green, blue, red, and yellow when gently rocked. The unique play-of-color pattern resembled broad, blocky brush strokes separated by areas of gray potch (figure 14). This array of iridescent colors was caused by light interacting with the silica spheres within the opal. However, the exact process behind the formation of such a distinct pattern is unknown, making this stone one of the more fascinating opals the author has encountered.

*Jessa Rizzo*

## PEARLS

### Assembled Bead Cultured Half-Pearl

Recently, the Carlsbad laboratory received for identification a loose, undrilled button-shaped item weighing 9.51 ct and measuring 12.56 × 12.45 × 8.87 mm (figure 15). This item appeared to be a typical mabe, the term for an assembled cultured shell blister, due to its composite nature and distinct seamline between a pinkish orange nacre dome top and a white mother-of-pearl shell base (figure 16, left). This type of assemblage is commonly manufactured from a thin nacre dome of a cultured shell blister cut from the shell surface with the half-dome implanted nucleus removed. Then the nacre dome is cleaned, filled, and sometimes colored with various kinds of artificial materials such as resin and backed with a piece of polished shell for stability.

Upon microscopic observation, the top dome portion appeared to be a thick nacre material due to the opaque-

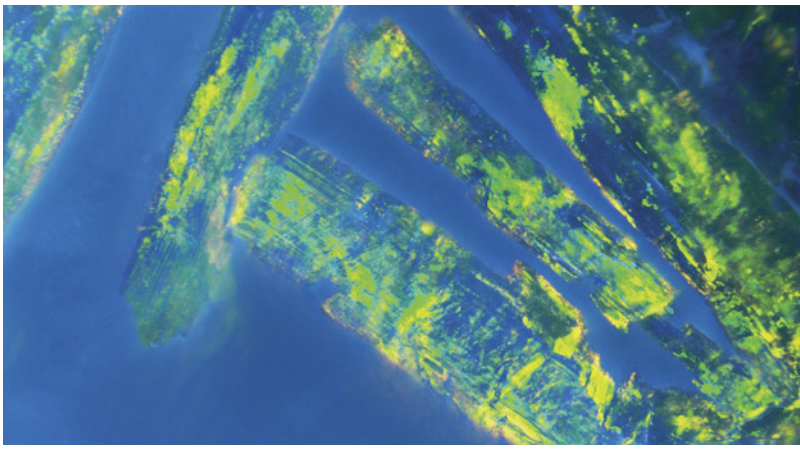

*Figure 14. Unique blocky brush strokes of play-of-color in the Australian black opal. Photomicrograph by Jessa Rizzo; field of view 7.19 mm.*

*Figure 13. A black opal cabochon displaying orange play-of-color when viewed face-up. Photo by Annie Haynes.*

*Figure 15. Assembled freshwater bead cultured half-pearl on an American freshwater shell. Photo by Rhonda Wilson.*

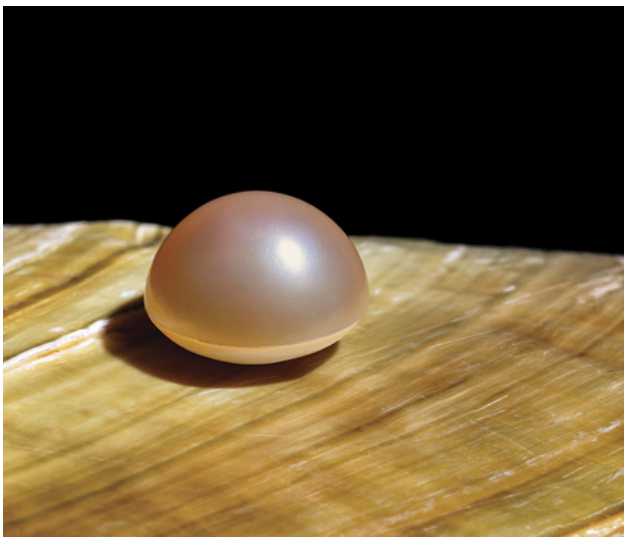

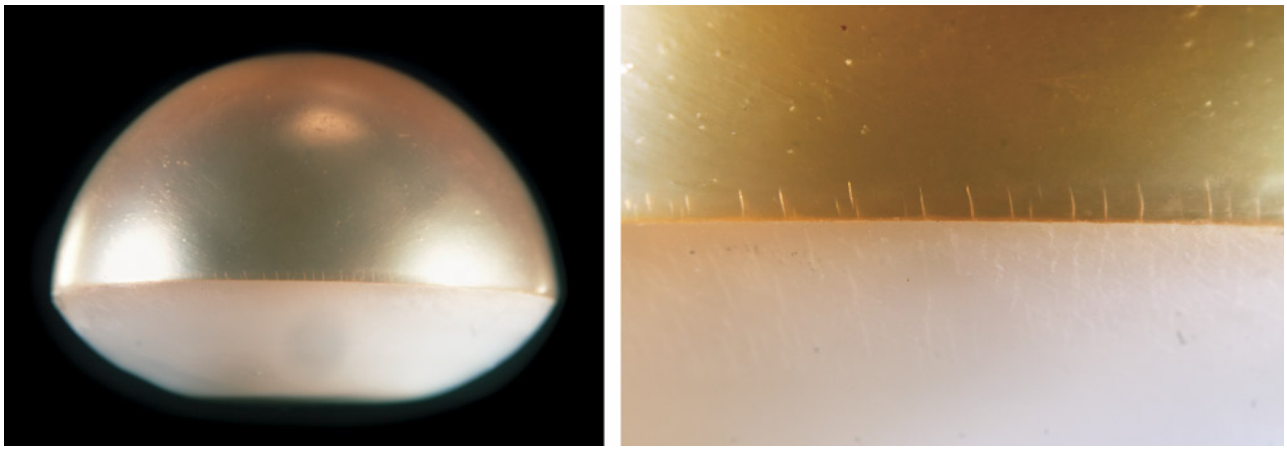

*Figure 16. Left: Side view of assembled freshwater bead cultured half-pearl showcasing the nacre dome top and shell backing. Right: Vertical fractures on the pinkish orange half. Photomicrographs by Kendra Carty; fields of view 16.57 mm (left) and 4.47 mm (right).*

ness of the nacreous surface, unlike the thin translucent nacre dome typically observed on most mabe materials. The surface contained common pits and scratches. However, many short vertical fractures were present within the surface of the top dome along the boundary (figure 16, right), an uncommon characteristic for mabe. The pinkish orange color appeared uniform, and a lack of unusual color concentrations suggested a natural color origin. This was subsequently confirmed with Raman spectroscopy using a 514 nm laser excitation, revealing two natural polyenic pigments at 1134 and 1526 $cm^{-1}$ along with aragonite peaks.

The boundary between the two sections was clearly visible in the real-time X-ray microradiography (RTX) image, and glue material appeared as bright radiopaque lines. Surprisingly, the top nacre dome had a thick nacre layer containing a few growth arcs within, and a semispherical demarcation of a bead nucleus (indicated by arrows in figure 17) was present. The structure resembled a typical bead cultured pearl. Further, the drilled bead nucleus, a common feature in freshwater pearls, suggested the bead cultured pearl was of freshwater origin (Summer 2017 Gem News International, pp. 255–256; A. Abduriyim, "Cultured pearls from Lake Kasumigaura: Production and gemological characteristics," Summer 2018 *G&G*, pp. 166–183). Energy-dispersive X-ray fluorescence chemical analysis of both the nacre dome top and shell base also indicated freshwater origin. The shell base showed a tight structure with very faint banding.

These findings indicated that the item was not a mabe as initially believed but rather an assembled freshwater bead cultured half-pearl. The vertical fractures shown under high magnification were likely caused by the sawing process (see again figure 16, right). This unique discovery was a first for GIA, demonstrating the importance of microradiography imaging in pearl identification.

*Amiroh Steen, Kendra Carty, and Artitaya Homkrajae*

## Enormous South Sea Cultured Pearl with Filled and Partially Hollow Structure

Many unusually large South Sea cultured pearls have been identified at GIA laboratories in the past (e.g., Fall 2013 Lab Notes, pp. 172–173; Summer 2023 Lab Notes, pp. 216–217). However, a recent submission to the New York laboratory particularly piqued the authors' interest. This submission featured a gigantic South Sea bead cultured pearl incorporated into a distinctive lariat necklace (figure 18).

The semi-baroque pearl measured approximately 31.00 × 28.07 × 27.24 mm and exhibited a silvery bodycolor with creamy patches, a common characteristic of pearls harvested from the *Pinctada maxima* oyster. Additionally, energy-dispersive X-ray fluorescence chemical analysis

*Figure 17. RTX image showing the half-pearl (top half) with a drilled bead indicated by arrows and shell backing (bottom half).*

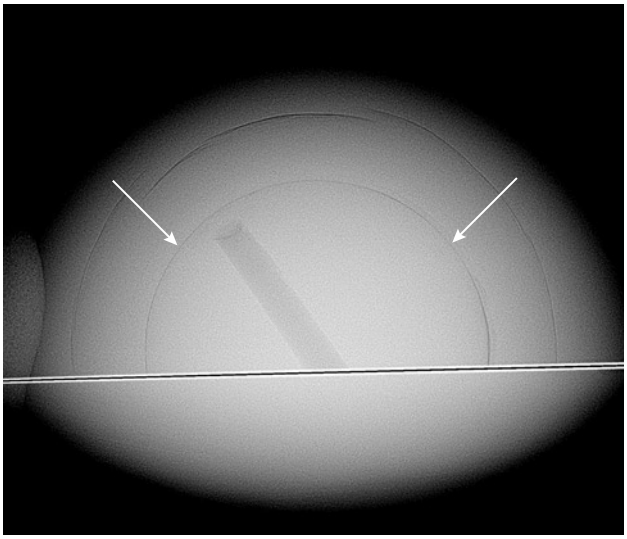

*Figure 18. A South Sea bead cultured pearl measuring approximately 31.00 × 28.07 × 27.24 mm set in a lariat necklace, shown alongside a typical 12 mm South Sea cultured pearl (right). Photo by Sood Oil (Judy) Chia.*

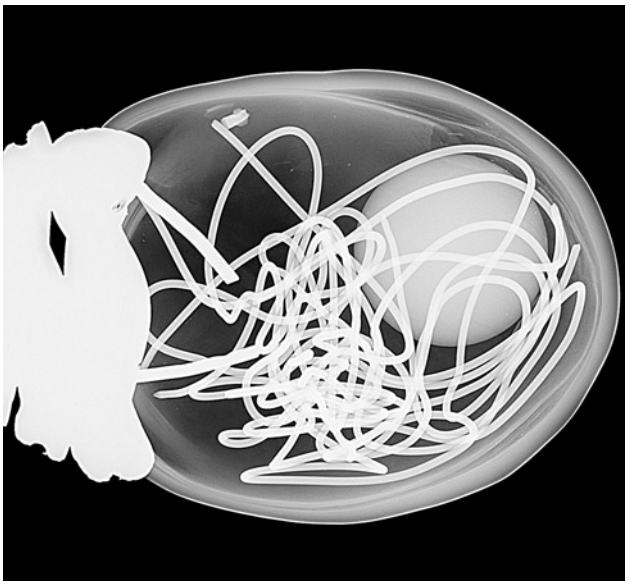

*Figure 19. RTX image showing a hollow structure filled with a round bead nucleus and multiple metal wires.*

showed low levels of manganese and high strontium content, confirming that the pearl originated from a saltwater environment.

This specimen represents one of the largest cultured pearls tested by GIA from the *Pinctada maxima* mollusk. *Pinctada maxima* is the largest species in the *Pinctada* genus, typically producing pearls ranging from 9 to 14 mm, though it sometimes produces exceptionally large pearls (L. Otter et al., "A look inside a remarkably large beaded South Sea cultured pearl," Spring 2014 *G&G*, pp. 58–62). Due to the pearl's size, it was fascinating to observe the internal growth structure. Real-time X-ray microradiography (RTX) imaging revealed a partially hollow structure containing a round bead nucleus approximately 10.5 mm in diameter, curiously filled with multiple metal wires approximately 0.40 mm in thickness (figure 19). The nacre thickness varied between approximately 0.50 mm to 1.00 mm.

Large pearls of either natural or cultured origin with hollow structures have occasionally been detected in laboratories, often filled with foreign materials such as resin, metals, shells, and even pearls (Fall 2013 Lab Notes, pp. 172–173; Spring 2014 Lab Notes, pp. 66–67; Summer 2019 Lab Notes, pp. 251–254). The observation of this large pearl filled with multiple metal wires was particularly interesting. Hollow pearls can be fragile due to their structural composition; the insertion of wires may serve to enhance durability, helping secure the bead in place, as well as retain weight.

This exquisite item was noteworthy for its size and intriguing internal structure. The lariat necklace featured a partially oxidized white metal set with numerous round brilliants gradually transitioning from near-colorless to gray and black, harmonizing with the beauty of the pearl.

*Emiko Yazawa and Joyce Wing Yan Ho*

## Natural Non-Nacreous Pearls from Various Marine Mollusks

GIA's Bangkok laboratory received for identification a set of 35 loose non-nacreous pearls displaying a wide range of bodycolors including white, orange, pink, brown, purple, and black. The pearls were near-round to round in shape and exhibited surface structure characteristics from various marine mollusk species (figure 20). Arranged in a necklace layout, they weighed from 3.96 ct to 51.63 ct and measured 8.40 × 8.01 mm to 19.20 × 18.93 mm (figure 21).

Observation with a 10× loupe and a microscope showed no evidence of color treatment on any of the pearls. Raman spectroscopy with a 514 nm argon-ion laser, as well as an 830 nm diode laser, was used to confirm color origin and examine the surface composition of all the pearls. The majority of the colored pearls displayed two main natural polyenic pigment peaks at 1120–1135 $cm^{-1}$ and 1505–1530 $cm^{-1}$, indicating their natural color origin. Real-time X-ray microradiography and energy-dispersive X-ray fluorescence analyses confirmed these were natural saltwater pearls.

Species determination was based mainly on the combination of colors and external appearances, internal growth structures, spectroscopic properties, and surface characteristics under magnification. Most of the pearls were porcelaneous and exhibited various flame structure patterns and high porcelain-like luster. All the white pearls were typical clam pearls produced from the Tridacninae subfamily. Under microscopic examination, many of the clam pearls displayed well-arranged flame patterns radiating from the centers (J-P. Gauthier et al., "Evidence of rotation in flame-structure pearls from bivalves of the Tridacnidae family," Summer 2019 *G&G*, pp. 216–228). The Melo pearls (from *Melo* species) were a yellowish

*Figure 20. A set of 35 non-nacreous pearls submitted for examination exhibited a variety of colors and surface structures, indicating they were formed by various mollusk species. Photo by Nuttapol Kitdee.*

orange color with visible flames that appeared to have jagged edges (Summer 2021 Lab Notes, pp. 152–153). Cassis pearls (from *Cassis* species) were present in various hues and saturations of light orange, pinkish orange, and

*Figure 21. The 35 near-round and round non-nacreous pearls, 482.01 carats total, arranged in a necklace layout. Photo by Nuttapol Kitdee.*


*Figure 22. Characteristic surface patterns observed on representative pearls produced from* Cassis *species in the necklace layout. A: Overlapping long, slender flame structures. B: Iridescent concentric rings observed slightly below the surface. C: Mottled surface structure with irregular streaks and patches. Photomicrographs by Kwanreun Lawanwong; fields of view 4.80 mm (A and C) and 2.88 mm (B).*

orangy brown. They shared characteristic long slender flames, some of which were overlapping (figure 22A). Iridescent concentric rings (Newton's rings) were also observed slightly below the surface of some Cassis pearls (figure 22B), similar to a previously reported feature (Fall 2012 Lab Notes, pp. 211–212). Another orangy brown Cassis pearl had a non-nacreous surface with a mottled appearance containing irregular streaks and patches but lacked any flame pattern (figure 22C; C. Zhou et al. "Disordered dolomite as an unusual biomineralization product found in the center of a natural Cassis pearl," *PLOS One*, Vol. 18, No. 4, 2023, article no. e0284295). Porcelaneous pearls from the Fasciolariinae subfamily (horse conch), *Aliger gigas* (conch; formerly known as *Strombus gigas* and *Lobatus gigas)*, and *Spondylus* species (thorny oyster) mollusk were also identified.

A group of scallop pearls from the Pectinidae family were identified in the collection. These pearls exhibited non-nacreous surfaces in the form of calcite, displaying a segmented patchwork of cells commonly found in scallop pearls and shells (figure 23, left). Some showed brownish purple and purplish brown colors typically produced by *Nodipecten* species, also known as the lion's paw scallop (K. Scarratt and H.A. Hänni, "Pearls from the lion's paw scallop," *Journal of Gemmology*, Vol. 29, No. 4, 2004, pp. 193–203). An additional black calcite pearl was concluded to be a pen pearl from the *Pinna* species. This pearl was semitranslucent and exhibited characteristic cellular surface structure (figure 23, right; N. Sturman et al., "Observations on pearls reportedly from the Pinnidae family (pen pearls)," Fall 2014 *G&G*, pp. 202–215; Winter 2014 Gem News International, pp. 305–306).

Finally, a few pearls in the collection exhibited borderline or unusual characteristics, and thus the producing mollusk species could not be determined. These included an orange pearl with a spiral surface pattern (see Micro-World, pp. 77–78 of this issue).

These pearls were likely produced in oceans and seas around the world, from the South China Sea to the Gulf of California (Sea of Cortez) and the Caribbean Sea. Finding a good-quality saltwater natural non-nacreous pearl is challenging, and the creation of this necklace layout required a great deal of effort and years of perseverance. The authors were grateful for the opportunity to examine this extraordinary set of pearls from a wide range of marine mollusk species.

*Areeya Manustrong, Ravenya Atchalak, Kwanreun Lawanwong, and Chunhui Zhou*

*Figure 23. Characteristic non-nacreous surface patterns observed on representative pearls produced from different mollusk species in the necklace layout. Left: Segmented patchwork of cells on a lion's paw scallop pearl (*Nodipecten *species). Right: Cellular structure and surface cracks on a pen pearl (Pinnidae family). Photomicrographs by Kwanreun Lawanwong; fields of view 7.20 mm (left) and 1.80 mm (right).*

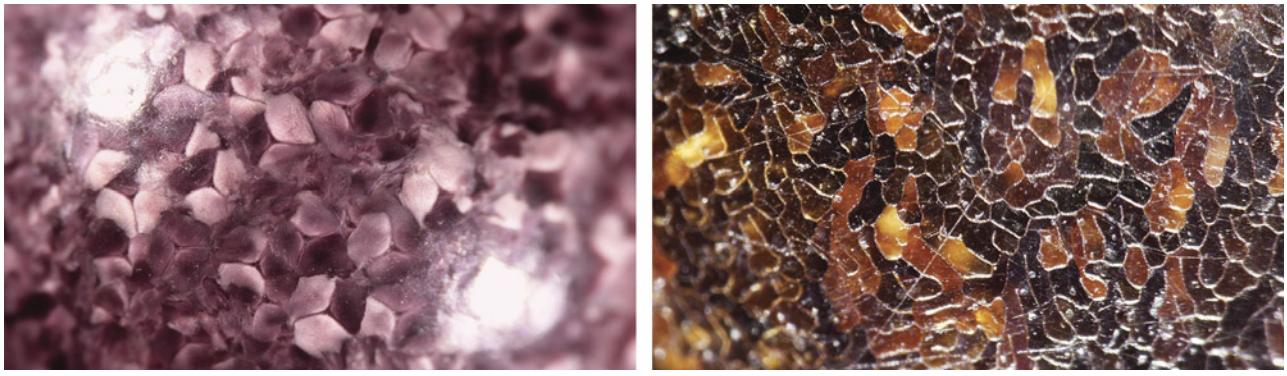

### Rock Crystal QUARTZ Skull

Recently, the Carlsbad laboratory received a remarkable sculpture for an identification report. The piece, named "Daath," was composed of two separate carvings: a skull weighing 3898.6 g and measuring 18.90 × 13.77 × 12.81 cm and an interlocking lower jawbone weighing 213.7 g and measuring 11.46 × 8.35 × 7.35 cm (figure 24). Microscopic examination revealed that both the skull and jawbone were doubly refractive and displayed natural fingerprints and fluid inclusions. The inclusion suite, in tandem with Raman spectroscopy, confirmed that both were carved from rock crystal quartz. A highly polished surface added to the brilliance of the sculpture.

Carved by Jarex Schmidt, the sculpture was completed over the course of four years. The carvings began as two pristine quartz crystals that were mined in 2014 from the Zigras mine in Blue Springs, Arkansas (figure 25). Rock crystal quartz is actively mined in the eastern portion of Arkansas, which is globally recognized for producing large, high-quality specimens suitable for carvings (https://www.geology.arkansas.gov/minerals/industrial/Quartz-(Industrial).html).

After more than 1,400 hours of meticulous hand carving and polishing, the quartz pieces were transformed into an extraordinary replica of a human skull. Realistic detail was captured with stunning accuracy and craftsmanship to create this one-of-a-kind carving.

*Jessa Rizzo and Nicole Ahline*

*Figure 25. Left: One of the rock crystal quartz crystals from the Zigras mine in Blue Springs, Arkansas, next to the skull the artist used as a reference for the sculpture. Right: The skull and jawbone components before more details were added. Courtesy of Jarex Schmidt.*

*Figure 24. "Daath," a 4112.3 g rock crystal quartz sculpture carved by Jarex Schmidt. Photo by Annie Haynes.*

## Irreversible Photochromism in SYNTHETIC SAPPHIRE

Recently, a 1.70 ct light blue stone was submitted as an alexandrite to the New York laboratory for identification (figure 26, left). Standard gemological testing yielded a refractive index of 1.760–1.768 and a specific gravity of 3.99, values consistent with corundum. Microscopic examination revealed an internally clean stone. It did not display curved color banding under diffused light, and Plato lines were not observed under cross-polarized light. Due to the lack of diagnostic inclusions and growth structures, the authors examined the stone's short-wave ultraviolet fluorescence under a mercury mineral lamp (S. Elen and E. Fritsch, "The separation of natural from synthetic colorless sapphire," Spring 1999 *G&G*, pp. 30–41). The stone displayed a moderately strong yellow "chalky" fluorescence with a banded pattern that is not known to be observed in natural stones. During the exposure time, which was only a few seconds, a photochromic effect occurred in which the bodycolor changed from light blue to yellow (figure 26, right). Photochromism can be defined as the reversible change of color from exposure to electromagnetic radiation, typically due to wavelengths of light from the visible to ultraviolet range.

Laser ablation–inductively coupled plasma–mass spectrometry returned very low concentrations of gallium (0.022–0.025 ppma), supporting a synthetic origin. The unnaturally high levels of nickel (28.3–31.2 ppma) may explain the sudden and drastic color change exhibited by this stone. In the late 1990s, researchers from the joint venture Tairus experimented with varying concentrations of $Ni^{2+}$, $Ni^{3+}$, and $Cr^{3+}$ to grow blue gem-quality hydrothermal sapphires with an even color distribution. Interestingly, some of their light greenish blue nickel-doped sapphires displayed a stable color change to yellow when artificially irradiated with gamma radiation (V.G. Thomas et al., "Tairus hydrothermal synthetic sapphires doped with nickel and chromium," Fall 1997 *G&G*, pp. 188–202). However, the sapphire studied here did not share the swirl-like growth observed in Tairus laboratory-grown sapphires.

Yellow and orange photochromism has been a known phenomenon in sapphires for some time (R. Crowningshield, "Developments and highlights at the Gem Trade Lab in New York: X-ray bombarded sapphires," Summer 1969 *G&G*, p. 57; K. Nassau and G.K. Valente, "The seven types of yellow sapphire and their stability to light," Winter 1987 *G&G*, pp. 222–231). Until now, however, changes in color with exposure to UV light have always been found to be reversible with exposure to white light.

The authors tried to revert the stone back to its original color, starting with the standard color stability test performed on all padparadscha sapphires submitted to GIA. This involves exposing the stone to a high-strength incandescent light source. When no change was observed, additional attempts were made, including gentle heating similar to that performed on "chameleon" diamonds, as well as X-ray exposure and long-term illumination under an LED light source containing no UV component. Images were collected before and after each stability test, and the bodycolor remained unchanged after every attempt to revert the stone to its original color. Despite these efforts, the sapphire was returned to the client as yellow.

This stone serves as a cautionary tale. Synthetic sapphire is often observed under short-wave UV or placed in a DiamondView to look for curved banding. Caution should be used when using these tests, at least on some colors of possible synthetic sapphire. To the authors' knowledge, this is the first documented case of corundum with irreversible photochromism encountered in a gemological laboratory. One should avoid exposing these pale blue laboratory-grown sapphires to UV radiation until this phenomenon is better understood.

*Axle Estrella and Tyler Smith*

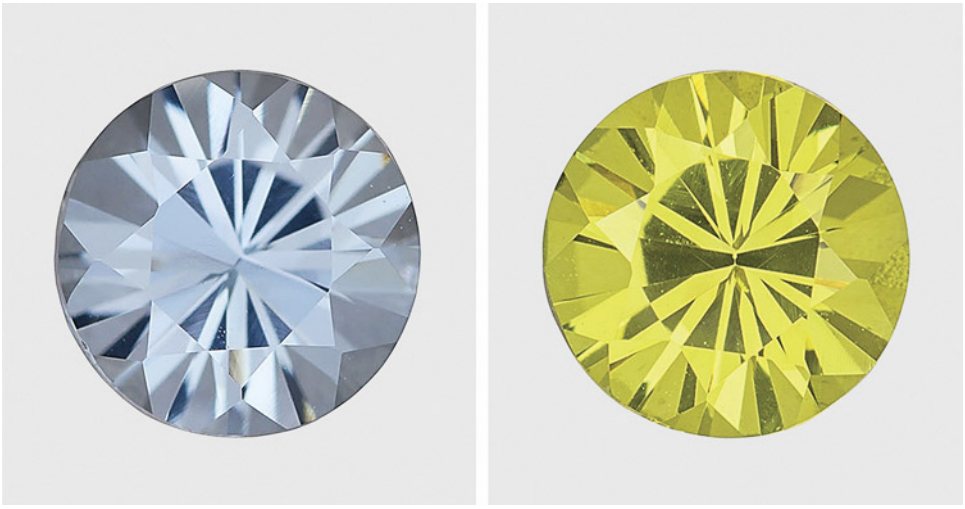

*Figure 26. Synthetic sapphire before (left) and after (right) exposure to short-wave ultraviolet radiation. Photos by Jian Xin (Jae) Liao (left) and Annie Haynes (right).*

## Rare Gem-Quality VIITANIEMIITE

The 4.86 ct near-colorless faceted gemstone measuring 10.56 × 8.63 × 7.31 mm shown in figure 27 was submitted to GIA's Bangkok laboratory for testing. The gemstone exhibited a refractive index ranging from 1.540 to 1.557, a biaxial negative optic nature, and a specific gravity of 3.10. When viewed in ultraviolet light, it displayed weak orange fluorescence under long-wave UV and strong yellow fluorescence under short-wave UV.

Raman spectroscopy confirmed the mineral's identity as the rare phosphate mineral viitaniemiite $Na(Ca,Mn^{2+})Al(PO_4)(F,OH)_3$ (A. Pajunen and S.I. Lahti, "The crystal structure of viitaniemiite," *American Mineralogist*, Vol. 69, 1984, pp. 961–966), with spectra matching the RRUFF viitaniemiite database entry (B. Lafuente et al., 2015, https://rruff.info/about/downloads/HMC1-30.pdf). Energy-dispersive X-ray fluorescence analysis detected high concentrations of phosphorus and calcium, along with aluminum and sodium, consistent with the phosphate composition of viitaniemiite. Microscopic examination revealed several notable internal features, including strong angular growth (figure 28, left), twinning, fingerprint inclusions, two-phase inclusions (figure 28, right), growth tubes, and tiny transparent crystals.

Viitaniemiite is known for its rarity and typically occurs in very small sizes in colorless, light blue, light green, and pale yellow hues within granitic pegmatites. The identification of viitaniemiite in a gemstone of this size was remarkable, given that the mineral is typically found in much smaller forms (S.I. Lahti, "On the granitic pegmatites of the Eräjärvi area in Orivesi, southern Finland," Geological Survey of Finland, Bulletin 34, Vol. 314, 1981, pp. 51–56). This discovery expands the known occurrences of viitaniemiite in gem-quality specimens and contributes valuable data to the gemological community.

*Figure 27. A 4.86 ct near-colorless faceted viitaniemiite. Photo by Lhapsin Nillapat.*

*Vararut Weeramongkhonlert*

*Figure 28. A rare gem-quality viitaniemiite shows angular growth (left) and a plane of irregular two-phase inclusions (right). Photomicrographs by Suwasan Wongchacree; fields of view 6.51 mm (left) and 2.32 mm (right).*